Theoretical Study of Lift-Generated Vortex Wakes Designed to Avoid Rollup

VERNON J. ROSSOW*
NASA Ames Research Center, Moffett Field, Calif.

Two hypothetical vortex wakes are introduced and studied theoretically to explore whether the rollup of lift-generated vortex sheets can be suppressed. The circulation distribution across each wake is specified such that one rotates and the other translates as a unit due to their self-induced velocities. Several span loadings are constructed from these solutions and the resulting inviscid wake structure is computed for several span lengths behind the generating wing by use of the discrete vortex method wherein the vortex wake is represented by an array of vortices. The final distribution of vortices is then used to estimate the rolling moment on an encountering wing. It is found that, even though the initial specified motions are not sustained, substantial reductions in rolling moment are predicted for certain ranges of the ratio of the span of the generating wing to the following wing.

Nomenclature

AR	= aspect ratio
b	= span of wing or vortex array
c	= chord
C_l	= rolling-moment coefficient = torque/$(\frac{1}{2}\rho U_\infty{}^2 Sb)$
C_L	= lift coefficient = lift/$(\frac{1}{2}\rho U_\infty{}^2 S)$
GAM	= dimensionless bound circulation or span loading = $\Gamma(y)/\Gamma_o$
$GAMR$	= dimensionless circulation in vortex = $\Gamma_v(R)/\Gamma_o$
N	= number of vortices in array that represents wake
r	= radius from center of vortex or from centroid of vorticity
R	= $2r/b_g$
t	= time
T	= $4t/\Gamma_o b_g{}^2$
u, v, w	= velocity components in x, y, and z directions
U, V, W	= $ub_g/2\Gamma_o$, $vb_g/2\Gamma_o$, $wb_g/2\Gamma_o$
x, y, z	= coordinate axes; x is streamwise and z is vertical
X, Y, Z	= $2x/b_g$, $2y/b_g$, $2z/b_g$
γ	= strength of vortex sheet = $-d\Gamma/dy$
γ_j	= circulation contained in jth vortex in array
$\Gamma(y)$	= bound circulation of wing
Γ_o	= centerline bound circulation for elliptically loaded wing

Subscripts

$\mathfrak{C}$	= centerline
f	= following wing that encounters wake
g	= wing that generates wake
v	= vortex
∞	= freestream

Introduction

THE vortices that trail behind lifting surfaces such as wings and helicopter rotor blades present undesirable and sometimes hazardous flow distortions to the lifting surfaces of aircraft entering that airspace. One solution is simply to avoid the regions occupied by these vortices. Alternatively, since it may not always be possible to locate and avoid vortices, it might be possible to change the nature of the wake of the vortex-generating aircraft or the roll performance of the encountering aircraft or both, so that acceptably safe flight can be sustained if vortices are encountered. The substantial increase in roll control required by current small aircraft to fly safely into the wake vortex of a large aircraft forces a consideration of methods for making the wake less hazardous. Past attempts to alleviate the vortex hazard include such methods as increased vortex diffusion by introducing turbulence into the vortex with generators (such as a wing-tip spoiler[1]), by acceleration of an instability,[2] or by shaping the wing to generate a vortex that has a less intense core.[3] A decrease in the lifetime or intensity of the vortices would presumably reduce the hazardous distance behind the generating aircraft. The optimal solution is achieved when aircraft spacing during landing and takeoff is determined by operational and safety considerations rather than wake turbulence. Naturally, any acceptable vortex alleviation scheme must also satisfy several practical constraints before the solution is usable. A fairly complete discussion and summary of the considerable literature on the structure of lift-generated vortices, some possibilities for their modification, and the effect a vortex might have on the motion of an encountering aircraft are given in a recent article by El-Ramly.[4]

Previous investigations[3,5-11] have considered the effect of wing planform shape or span loading on the vortex structure but none have designed the wing for a specific wake-vortex structure. The work presented here is based on the premise that vortex wakes do not necessarily need to roll up into the familiar concentrated vortices associated with elliptically loaded wings. An attempt is made here to suppress the rollup process by specifying the circulation distribution in two idealized wakes so that their shape does not change with time. The wake motion is then studied to determine whether these hypothetical wakes are effective in alleviating the hazard.

Received November 14, 1973; revision received October 7, 1974.
Index categories: Aircraft Aerodynamics (Including Component Aerodynamics); Jets, Wakes, and Viscid-Inviscid Flow Interactions; Aircraft Flight Operations.

* Staff Scientist. Associate Fellow AIAA.

I. Analysis

A. Initial Configuration of Wakes Designed to Avoid Rollup

The analysis of complete aircraft wakes including the contributions of the fuselage, landing gear, etc., is idealized here by assuming that the wake is inviscid and dependent only on the span loading, $l(y) = -\rho U_\infty \Gamma(y)$, of the wing that generates the wake. Figure 1 illustrates, for an elliptically loaded wing, the conventional relationships between the bound circulation on the wing, $\Gamma(y)$, and the vortex sheet represented by $\gamma(y) = -d\Gamma(y)\,dy$, that rolls up into two spiral-shaped cores. Also shown for the right wing only is the fully developed vortex that results far downstream from the lifting surface. The wake motions are also assumed to be changing slowly enough in the streamwise direction that they can be treated as two-dimensional, unsteady wakes in the so-called Trefftz plane (Fig. 1), and that the vorticity distribution can be represented by a distribution of point or discrete vortices (see Appendix for discussion of this technique).

When the centers of the vortices that represent the wake lie on a line so that the array is flat or planar, two velocity distributions yield vortex wakes that move as a unit without changing shape.

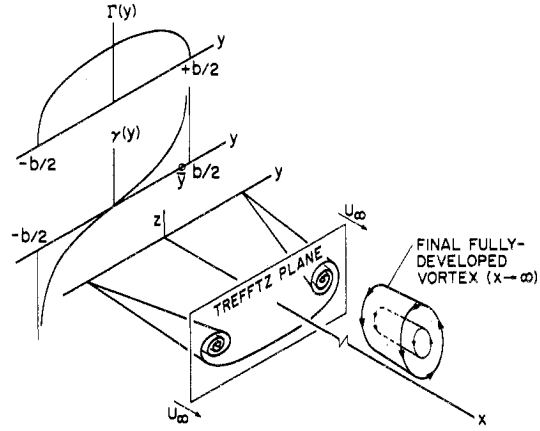

Fig. 1 Schematic diagram of relationship between span loading $\Gamma(y)$, vortex sheet, $\gamma(y)$, Trefftz plane, and final rolled-up vortex for one side.

These two motions are illustrated in Fig. 2 by two arrays of vortices that move in rotation and translation. Consider first the initial motion of the planar arrays with no specification made as to the stability of the motion. The velocity components are

$$v_i)_{t=0} = 0 \tag{1a}$$

$$w_i)_{t=0} = \sum_{j\neq i}^{N} \frac{\gamma_j}{2\pi(y_i - y_j)} = \begin{cases} \Omega y_i \text{ for rotation} \\ w_o \text{ for translation} \end{cases} \tag{1b, 1c}$$

where v and w are the velocity components in the y and z directions, γ_j is now the strength of the jth vortex in the array, and N is the number of vortices. The angular velocity of the rotating array is Ω and the translating velocity is w_o. The vortices are assumed to be spaced uniformly along the y axis at $t = 0$. Since the location and velocity are known for every vortex in the array, and the vortex strengths are unknown, a sequence of equations is written using Eqs. (1). The resulting matrix is inverted numerically on an electronic computer to yield the strengths of the vortices.† The span-load distributions that correspond to these arrays are then found by integrating the relationship $\gamma(y) = -d\Gamma(y)/dy$.

The strengths of 20 vortices in an array designed to rotate at 1 rad/unit time and for an array designed to translate downward at 1 spanlength/unit time are shown in Figs. 3(a) and 3(b). Figure 3(b) also shows the strengths of the vortices shed by an elliptically loaded wing designed to also have an initial downward motion of 1 spanlength/unit time. The vortices in the rotating array have the same sign and the variation in strength across the span of the array is approximately elliptical. The vortex strengths in the translating array do not vary smoothly but alternate from positive to negative. The vortex strengths shed by elliptic loading vary smoothly but the wake motion differs. All center vortices move downward together whereas the two end vortices now move upward, causing the wake to roll up into a single vortex pair. To compare the merits of the rotating and translating wakes with the wakes of conventional span loading, the strengths of the vortices are adjusted in the following sections

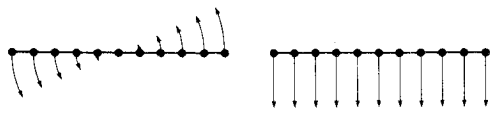

Fig. 2 Two vortex arrays designed to move as a unit without rolling up. a) Solid-body rotation, $w = \Omega y$; b) uniform downward velocity, $w = \text{const}$.

† The subroutine used to invert the matrix is an improved double-precision linear equation solver developed by R. T. Medan of Ames Research Center.

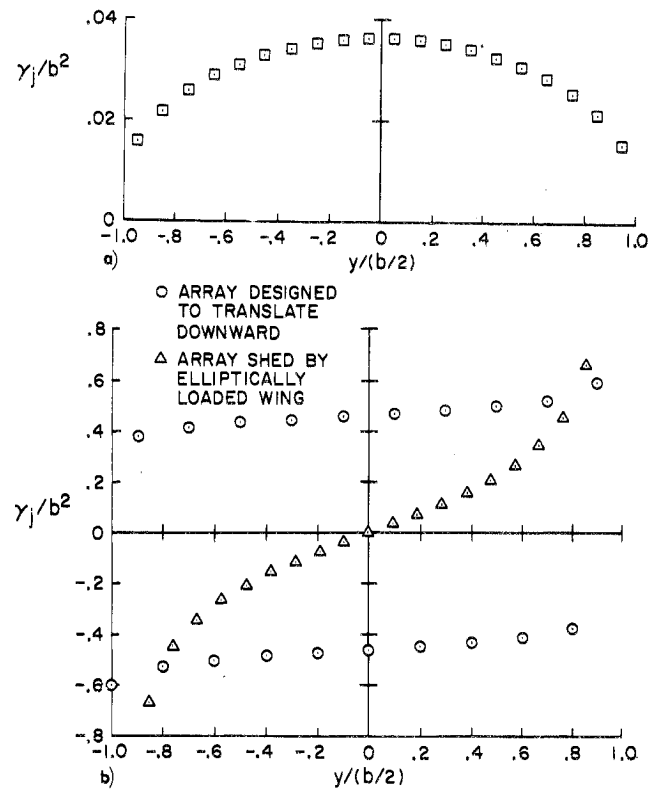

Fig. 3 Structure of hypothetical arrays. a) Strengths of the 20 vortices in an array designed to rotate as a unit at 1 rad/unit time; b) vortex strengths for translating array and for elliptically loaded wing; both are designed to move downward at 1 span/unit time. Values for tip vortices at $\gamma_1/b^2 = -\gamma_{21}/b^2 = -1.34$ are off scale for elliptic loading.

so that the span loading yields the same lift as an elliptically loaded wing.

B. Numerical Method for Subsequent Structure of Wake

The method used to calculate the motion of the vortices in the arrays is similar to that used in previous investigations of the structure of lift-generated wakes.[5-8,12-17] Discussions in Refs. 13–21 treat the shortcomings and limitations of this approach. The Appendix summarizes these discussions, describes the precautions taken to avoid numerical errors in the calculations, and presents an approximate scheme for estimating the rolling moment on aircraft that encounter wake vortices. The vortex motions predicted below are, within plotting accuracy, free of numerical error.

In the following calculations, the three-dimensional effects of the bound vortex and the termination of the trailing vortex at $x = 0$ are ignored. Since any influence of a fuselage, tail, etc., on the vortex motion is also ignored, the results are to be interpreted as trends rather than as numerically exact representations of the wakes of aircraft. With these simplifications, the expressions used to predict the motion of the individual vortices in the wake are

$$v_i = \frac{\Delta y_i}{\Delta t} = -\sum_{j\neq i}^{N} \frac{\gamma_j(z_i - z_j)}{2\pi[(y_i - y_j)^2 + (z_i - z_j)^2]}$$

$$w_i = \frac{\Delta z_i}{\Delta t} = +\sum_{j\neq i}^{N} \frac{\gamma_i(y_i - y_j)}{2\pi[(y_i - y_j)^2 + (z_i - z_j)^2]}$$

The locations of the N vortices at an advanced time were found by using velocity averages over the time increment Δt. Since the final positions of the vortices affect the calculated velocities, it was necessary to iterate about five times for the new locations. To estimate the numerical errors that may occur during a calculation, the Kirchhoff-Routh path function[22] and the first and second moments of circulation for each side of the wing

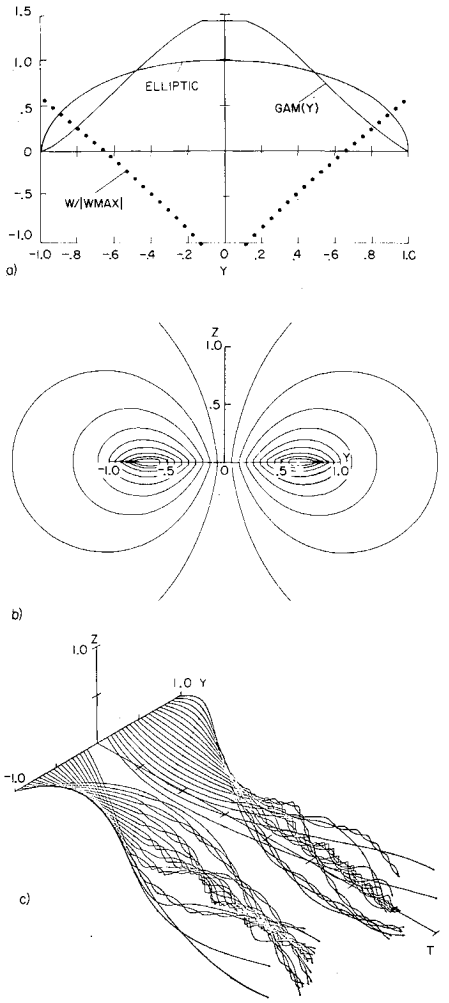

Fig. 4 Flow characteristics for span loading built with two arrays designed to rotate as a unit; 90% tailored. When $b_g/b_f = 2$, $C_{l_f}/C_{L_g} = 1.06/\mathcal{A}R_g$. a) Spanwise loading and downwash velocity at $x = 0$; b) streamlines in Trefftz plane at $x = 0$; c) oblique view of vortex paths, $T_{max} = 3.0$.

were monitored during the calculations (see Appendix). The results presented in the figures that follow are then such that the numerical errors indicated by the error monitors are less than plotting accuracy.

For comparison, the bound circulation or span loading for the various cases to follow are normalized so that they represent the same lift as an elliptically loaded wing. The bound circulation for elliptic loading is therefore included in the various figures. The total lift on the generating wing is

$$C_{L_g} = \mathcal{A}R_g(\Gamma_o/b_g U_\infty)\int_{-1}^{+1} GAM(Y)\,dY$$

where $GAM(Y) = \Gamma(Y)/\Gamma_o$ and Γ_o is the circulation shed by one side of an elliptically loaded wing at the lift coefficient C_{L_g}. The dimensionless bound circulation or span loading on the generating wing is then normalized so that $\int_{-1}^{+1} GAM(Y)\,dY = \pi/2$. Other dimensionless parameters used in the analysis are defined in the nomenclature list.

II. Application of Hypothetical Wakes to Wings

A. Tailored Span Loading for Rotating Wakes

The strengths of the vortices in the rotating array [Fig. 3(a)] have the same sign so that one such array can represent the wake shed by only one side of the wing. A second array identical in all respects but opposite in sign must then be used to represent the wake shed by the other half of the wing. The space allowed between the two arrays is arbitrary and that part of the span has uniform loading at the centerline value. Since each array can occupy part or all of the semispan by varying the gap size, the wing planform, twist, or camber, the loading is considered to be tailored over a certain percentage of the span to produce a rotating array from each half of the wing; that is, a wing tailored 40% would shed a vortex sheet from the outer 40% of each side of the wing. Since the arrays were specified to rotate when they were isolated, one purpose of the numerical calculations is to determine how the presence of the second array affects the rotational motion.

Figure 4 presents the calculated vortex wake structure for a case when two rotating arrays of opposite sign are added to form a loading tailored 90% of the wing span. The span loading, the induced velocities for the vortices or the downwash [Fig. 4(a)], and the streamlines for the $x = 0$ plane [Fig. 4(b)] indicate the nearly triangular nature of the span loading and the downwash. The presence of the second array distorts the linear variation in the initial vortex velocity profile only slightly near the centerline of the wing even for the loading tailored 90%. The streamlines in the Trefftz plane at $x = 0$ close on the wing itself rather than looping over the wing tip as occurs with elliptically loaded wings [cf. Fig. 9(b)]. Figure 4(c) shows that the two vortex arrays that were designed to rotate separately interact enough to modify the uniform rotation after only a partial revolution. If the initial conditions for pure rotation are disturbed further by displacing a vortex from the y axis at $T = 0$, the orderly part of the rotation is affected sooner, but the wake structure at the final time does not appear to be significantly different from that shown in Fig. 4(c). If the gap between the two rotating arrays is increased from 10% of the span, the arrays rotate more independently; however, the vorticity is then spread over a smaller part of the span, resulting in a concentration of vorticity. The effect of gap size or tailoring on the induced drag is presented in Fig. 5. The value for an elliptically loaded wing ($C_{D_i} = C_L{}^2/\pi\mathcal{A}R_g$) is used as the reference. As expected, an induced drag penalty occurs when tailored loadings are used if the comparison is made on the basis of span efficiency.

Note that if the tailored loadings are obtained by shaping the planform of the generating wing, the shapes resemble the ogee wing tips suggested by J. Ward and studied in Refs. 3 and 9. The objective of these wing-tip shapes was to reduce the velocity in the vortex and thereby reduce the noise of helicopter rotor blades.

Continuous tailored vortex sheet

When the number of vortices in the rotating array is allowed to increase indefinitely, the vorticity distribution becomes continuous and is given by

$$\gamma(y) = -[(d\Gamma(y)/dy)] = \pm(4\Gamma_{\mathcal{C}}/\pi b)[1-(2y/b)^2]^{1/2}$$

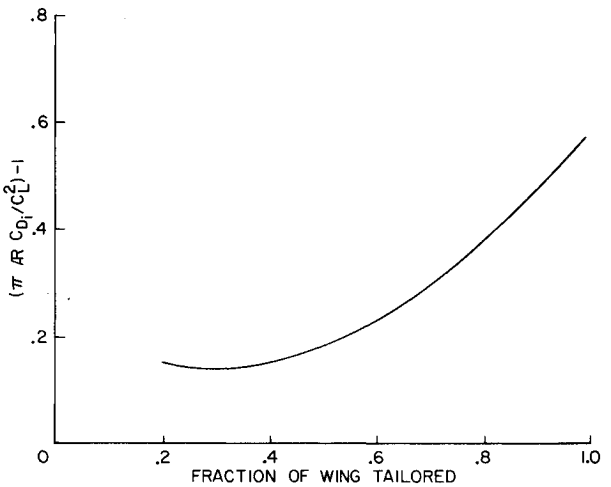

Fig. 5 Induced drag for wings with tailored loading.

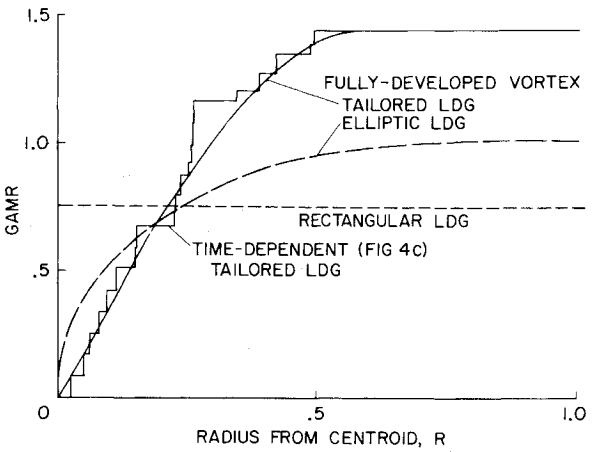

Fig. 6 Radial distribution of circulation in wake vortices shed by 90% tailored loading as predicted by time-dependent method [see Fig. 4(c)] and by Betz' theory for fully developed vortices.

and the circulation (proportional to span loading) is

$$\Gamma(y) = \Gamma(-b/2) + (\Gamma_{\text{℄}}/\pi)\{(2y/b)[1-(2y/b)^2]^{1/2} + \sin^{-1}(2y/b) + \pi/2\}$$

where b is now the span of the vortex sheet and $\Gamma_{\text{℄}}$ is the total circulation in the sheet. These two functions are the limiting forms of the elliptic distribution derived by Lamb (p. 232)[24] to rotate as a unit, and studied by Kuwahara and Takami[20] using discrete vortices. These relationships are now used to calculate the structure of the fully developed vortex (i.e., Betz' theory). From Eq. (17) of Ref. 11, the radius in the vortex that contains a given amount of circulation may be written as

$$2r/b = Y - 2\Gamma_{\text{℄}}\,[(1-Y^2)^{1/2}-1]/\{3\pi[\Gamma(Y)-\Gamma(0)]\}$$

where $Y = 4\{y-[1-(T_t/2)](b/2)\}/T_t b$ and T_t is the fraction of the wing that is tailored. The circulation $\Gamma_v(r)$ contained in the vortex at the radius r is then

$$\Gamma_v(r) = 2\Gamma(y)$$

because the vortex sheet rolls up about its center. The center of the vortex is located at the spanwise location of the center of the tailored wing segment because that is the centroid of vorticity for a side. The circumferential velocity is given by

$$v_\theta = [\Gamma_v(r)/2\pi r]$$

The circulation in the fully developed vortex calculated from these equations for the tailored vortex sheet is compared in Fig. 6 with the radial variation of circulation from the center of gravity determined by the time-dependent calculations at dimensionless time $T = 3.0$ The parameter $GAMR = \Gamma_v(2r/b_g)/\Gamma_o$ is determined with the technique described in the Appendix. Some of the differences between the two results are attributable to the finite time used in the time-dependent result and to the fact that the Betz theory ignores the interaction of vortices shed by the other half of the wing.

Rolling moment on wing in wake of tailored loading

A simplified method is described in the Appendix for estimating the torque on a wing with a rectangular planform whose center is coincident with the centroid of vorticity for one side of the wake. The circulation distribution used to evaluate the torque is obtained from the time-dependent calculations in Fig. 4(c) at dimensionless time $T = 3$, which is about three spans behind the generating wing. The point-vortex distribution is first reinterpreted in terms of an axially symmetric vortex as explained in the Appendix. Figure 6 compares the data for the 90% tailored case with the vortex shed by rectangular and elliptic loading. Equation (A5) expresses the fact that the area under the curve of $GAMR$ (or $\Gamma_v(R)/\Gamma_o$) vs R to a given radius is proportional to the rolling moment on a wing located at the center of the vorticity or centroid. Comparison of the areas under the three curves in Fig. 6 for various radii indicates that the tailored loading produces the smaller rolling moment for $b_g/b_f \gtrsim 4$ (corresponds to $R \lesssim 0.25$ in Fig. 6). However, as the span of the follower increases, the advantage of tailored loading disappears so that, for $b_g/b_f = 2$, the hazard parameter becomes $C_{l_f}/C_{L_g} = 1.06/\mathcal{R}_g$ compared with $1.0/\mathcal{R}_g$ and $0.9/\mathcal{R}_g$ for rectangular and elliptic loading, respectively. Hence, even though the peak velocity is probably reduced in the vortex, the dispersion of vorticity by tailoring is not enough for the larger following wings to offset the increased centerline circulation needed to retain a given lift on the generating wing.

The range of span ratio where tailoring is advantageous cannot be enlarged because shaping more than 90% of the span loading is probably not feasible because part of the span is occupied by the fuselage. Conversely, a decrease in the amount of tailoring tends to concentrate the circulation in the vortex. Therefore, the range of span ratio over which tailoring is beneficial shrinks as less of the span loading is devoted to the vortex sheet. The foregoing approximate calculations therefore indicate that reduced rolling moments are expected when the span of the following wing is small compared to that of the generating wing.

B. Stepped Span Loading for Translating Wake

The vortices for a translating array [Fig. 3(b)] are both positive and negative in sign and sum to zero circulation so that a single array can be used to represent the entire wake of a lifting wing. When the vortex distribution [Fig. 3(b)] is integrated for the bound circulation (or span loading) on the wing, the discontinuous or stepped curve shown in Fig. 7(a) is obtained.

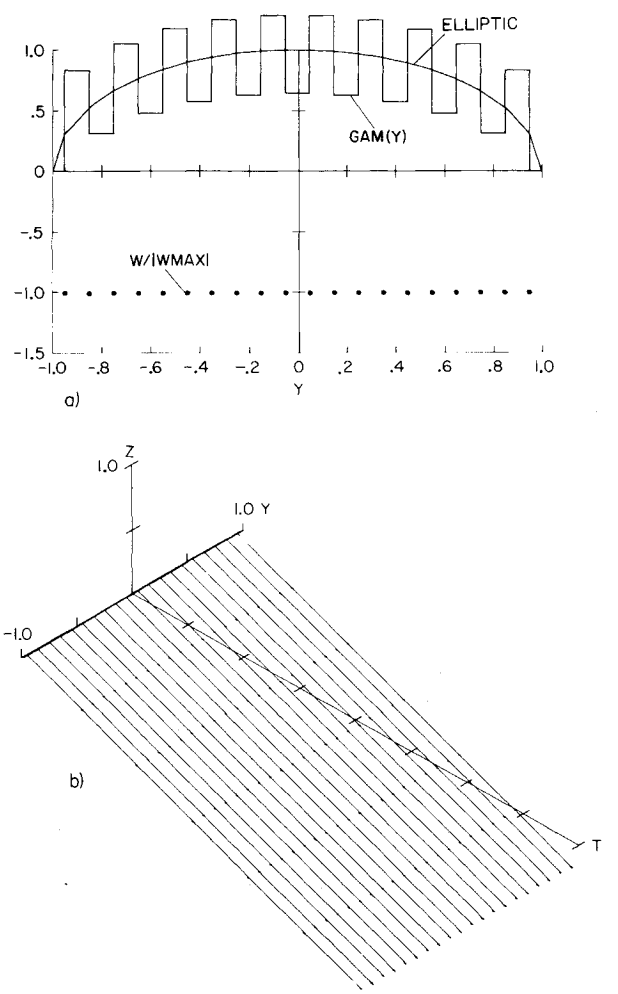

Fig. 7 Characteristics of span loading built with array designed to translate as a unit. When $b_g/b_f = 2$, $C_{l_f}/C_{L_g} = 0.34/\mathcal{R}_g$. a) Span loading compared with elliptic loading and downwash velocity of each vortex in the array; b) oblique view of shape of vortex lines; $T_{max} = 3.0$.

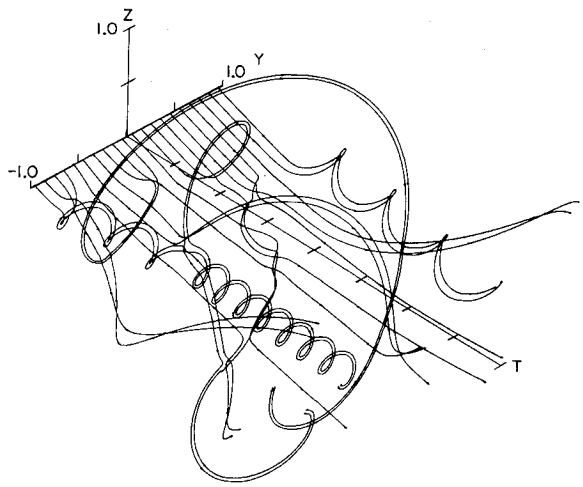

Fig. 8 Vortex motion of translating array when initial position of fifth vortex is displaced $0.01b_g/2$. Note how vortices form pairs that move along circular paths that deviate occasionally to exchange mates; $T_{max} = 3.0$. When $b_g/b_f = 2$, $C_{l_f}/C_{L_g} = 0.03/\mathcal{R}_g$.

Such a loading could be interpreted as an approximation to the loading achieved by deflecting the flaps upward and downward alternately across the span. As expected, the specified downward motion of the vortices in the array is achieved when the time-dependent calculations for the wake isolated from other vortices and when the flow conditions are uniform. The individual vortices therefore appear as straight lines that trail from the lifting line at $x = 0$ as shown in Fig. 7(b). If, however, the initial condition of one of the vortices is disturbed (e.g., by displacing the fifth vortex a small amount vertically), the specified motion breaks down into the chaotic motion‡ shown in Fig. 8. The erratic motions change to a new pattern if another disturbance is used.

The nearly circular paths of the various pairs of vortices appear to arise from the fact that two vortices of opposite sign and of unequal magnitude form a pair. That combination then moves along a path whose radius of curvature R is governed by the velocity induced by the two vortices on each other:

$$R = d(\gamma_l - \gamma_r)/[2(\gamma_l + \gamma_r)]$$

where d is the distance between the two vortices and γ_l and γ_r are the strengths of the left and right vortices, respectively. The orbits of the various pairs of vortices are governed by all the vortices in the wake, but the proximity of any two causes their particular motion to depend largely on the circulation they possess. The magnitude and type of disturbance influence how the vortices match to produce the chaotic motion. Since the uniform translating motion was destroyed by a small perturbation, and since the flow disturbances behind an aircraft in flight are of a wide variety and magnitude, the detailed motions presented here indicate trends and should not be considered directly applicable to a given case.§

The dispersion of the vortices (Fig. 8) and the numerical value for the hazard parameter indicate that the rolling moment on an encountering aircraft can be reduced substantially if the chaotic vortex motions are achieved in practice. The discontinuous character of the span loading suggests that the vortex sheet behind such a lifting surface quickly becomes an array of vortices instead of a continuous sheet. Therefore, the numerical results calculated for the array should not be reinterpreted for a continuous sheet.

C. Combination of Two Stepped Loadings for Elliptic Loading

Previously, a closed-form solution was presented for the rotating array when the number of vortices N became infinite. A similar result could not be found for the array that translates as a unit because the amplitude of the steps in the vortex strengths appears to decrease only slightly as N increases. However, a continuous loading is achieved if two arrays equal in number and in strength are superimposed so that one array is offset from the other by one vortex spacing. The loading is then elliptical with the characteristic downwash velocity being uniform everywhere except at the two ends, where it is discontinuous. Figure 9 presents the calculations for such a case. As expected, rollup proceeds rapidly and orderly from the wing tips inboard. If an initial displacement is given to one of the vortices in such an array, the rollup proceeds almost unchanged—a very different response from that obtained for the stepped loading.

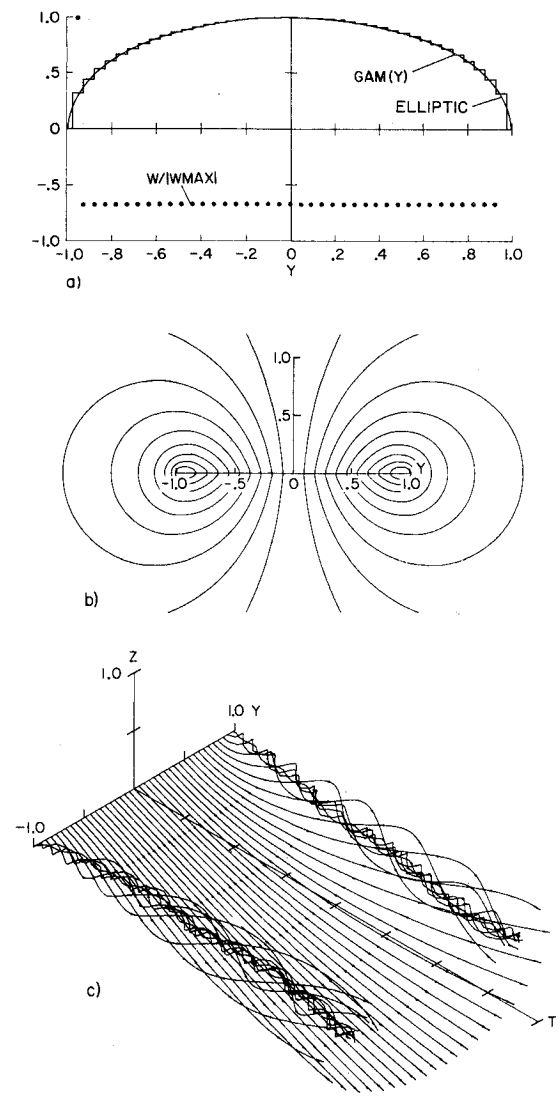

Fig. 9 Characteristics of span loading obtained by adding two translating arrays after shifting them one vortex spacing spanwise. This loading quickly approximates elliptic loading as the number of vortices N is increased. When $b_g/b_f = 2$, $C_{l_f}/C_{L_g} = 0.87/\mathcal{R}_g$. a) Span loading of the combined translating arrays shown as stepped curve compared with elliptic loading and velocity of vortices at $x = 0$. Note the two vortices at the ends of the array with greatly different velocities; b) streamlines in Trefftz plane at $x = 0$; c) oblique view of vortex paths; $T_{max} = 3.0$.

‡ The use of vortices with artificial viscous cores (suggested by Chorin and Bernard[19] and by Kuwahara and Takami[20]) instead of the potential vortices used here stabilizes and smooths out the vortex motion. However, it does not alter the qualitative nature of the solutions when the core radius is less than the initial vortex spacing. Since the character of these calculations is not greatly different, the viscous core results are not included.

§ The induced drag for these loadings was not estimated because of their discontinuous character.

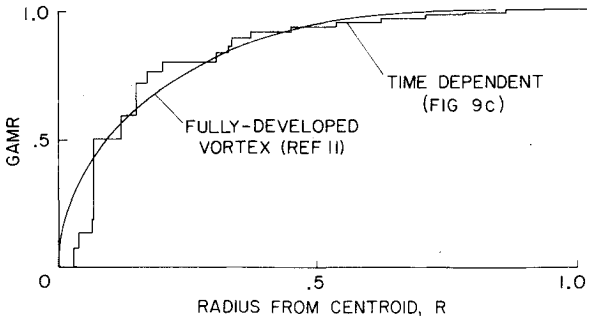

Fig. 10 Circulation in wake vortices shed by elliptic loading as predicted by time-dependent method [see Fig. 9(c)] and by Betz' theory for fully developed vortices.

The variation of the circulation with radius from the centroid of vorticity given by the time-dependent results in Fig. 9(c) is compared in Fig. 10 with the structure predicted by Betz' theory for a fully developed vortex shed by an elliptically loaded wing tip.[11] As with the tailored loading case (Fig. 6), the agreement between the two results is good, considering that the approximations made in the two theories are quite different.

D. Combination of Tailored and Stepped Span Loadings

If the span loading for an array that rotates uniformly is added to one that translates as a unit, the question arises as to what proportion of each should be used in the mixture to develop a chaotic wake. Therefore, several computer runs were made in which the proportion of stepped loading (i.e., translating array) was increased until a somewhat random wake was achieved in the 90% tailored case. Figure 11 presents the case for 40 vortices wherein more than enough of the stepped loading has been added to randomize the wake of the tailored loading (rotating array). Since no effort was made to optimize the step size and number, the results in Fig. 11 are intended only to illustrate the type of wake obtained when rotating and translating wakes are mixed.

E. Sawtooth Span Loading

The magnitude of the vortex strengths in the array that translates as a unit has been calculated precisely and used in this form. Since such precision is difficult to achieve in experiments, another sawtooth type or discontinuous loading is considered. Since the stepped loading is approximated by an elliptic loading plus the loading of an array of vortices equal in magnitude but alternating in sign, the motion of vortices in such an array is studied. Figure 12 presents the span loading and vortex motion that result from such an array. As expected, the wake becomes random. For convenience, this array is referred to as sawtooth loading, whereas that of the translating array is called stepped loading. Furthermore, randomization of the vortex wake again occurs when a sawtooth loading is added in about the same proportion as the stepped loading to the 90% tailored loading. The proportion of stepped or sawtooth loading required to randomize the wake vortex system of a given span loading is not necessarily a well-defined amount; rather the randomness seems to increase rapidly after the sawtoothing has increased above a certain amount or fraction of the centerline circulation.

F. Combination of Sawtooth and Aircraft Span Loadings

An attempt is made here to apply the results of the previous sections to the span-load distribution of typical, current, large aircraft. The span loading chosen for this example and the estimated motion of the wake vortices that represent the wake

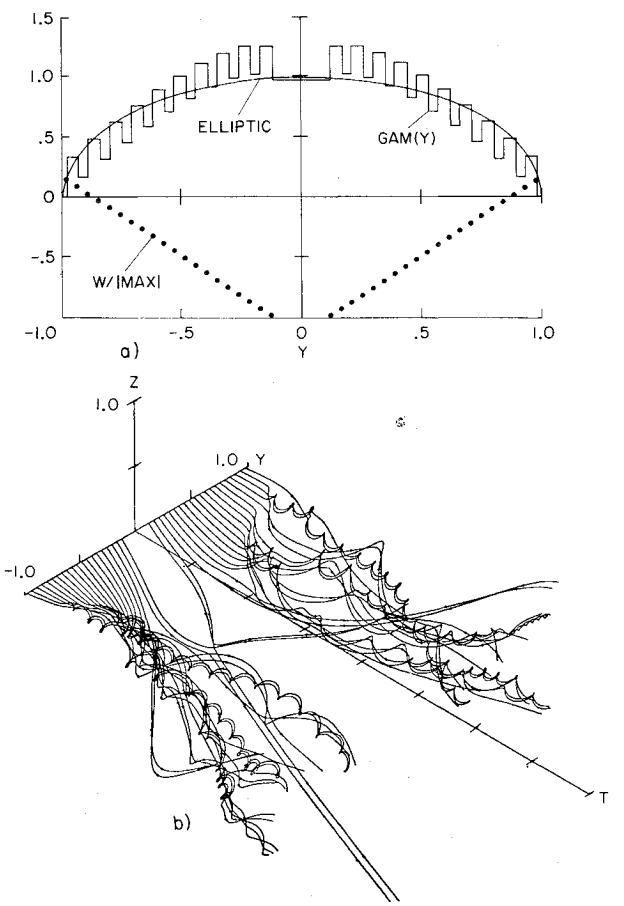

Fig. 11 Characteristics of span loading obtained by combining a translating array with a rotating array. Translational velocity = $(0.6b_g/4)$ × rotational velocity. When $b_g/b_f = 2$, $C_{l_f}/C_{L_g} = 0.02/\mathcal{R}_g$. a) Span loading and velocity of vortices at $t = 0$; b) oblique view of vortex paths; $T_{max} = 2.4$.

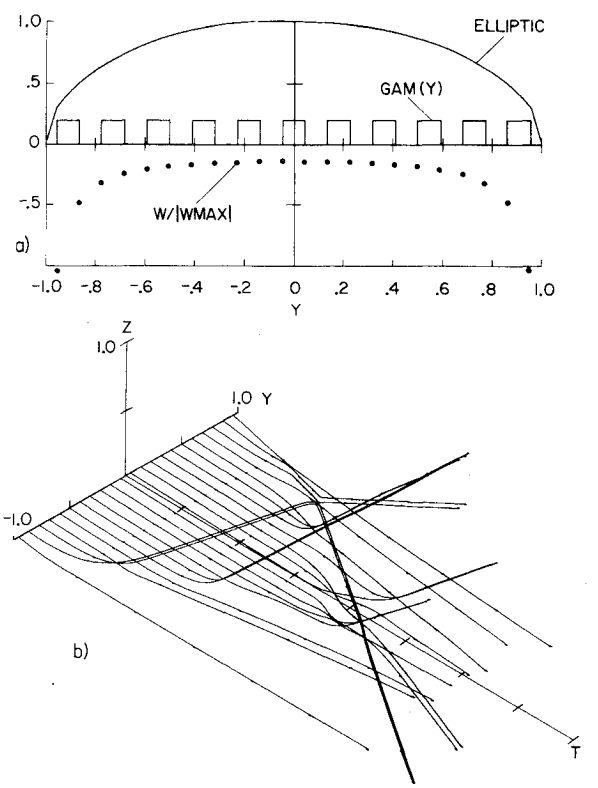

Fig. 12 Characteristics of sawtooth loading formed by vortices equal in strength but alternate in sign. a) Span loading compared with elliptic loading and downwash velocity of vortices at $t = 0$; b) oblique view of vortices; $T_{max} = 3.0$.

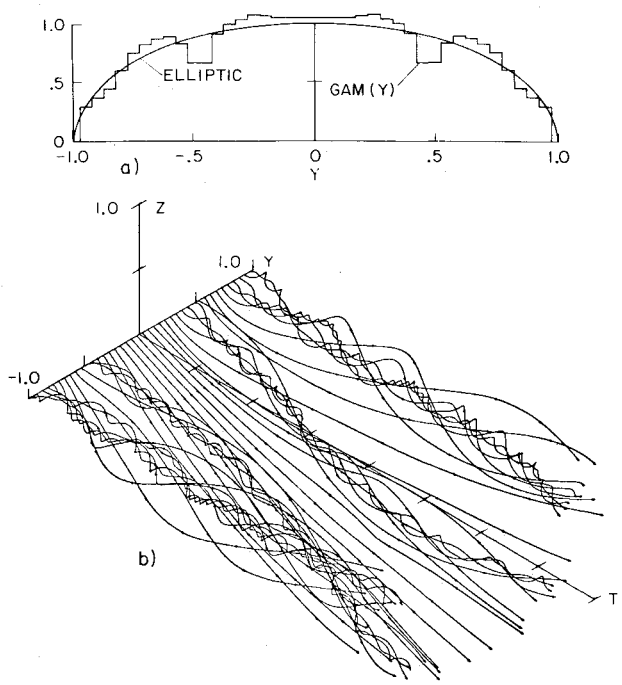

Fig. 13 Characteristics of loading typical of current large aircraft in landing configuration. When $b_g/b_f = 2$, $C_{l_r}/C_{L_a} = 0.75/\mathcal{R}_g$, a) Vortex array approximation to span loading; b) oblique view of vortices; $T_{max} = 3.0$.

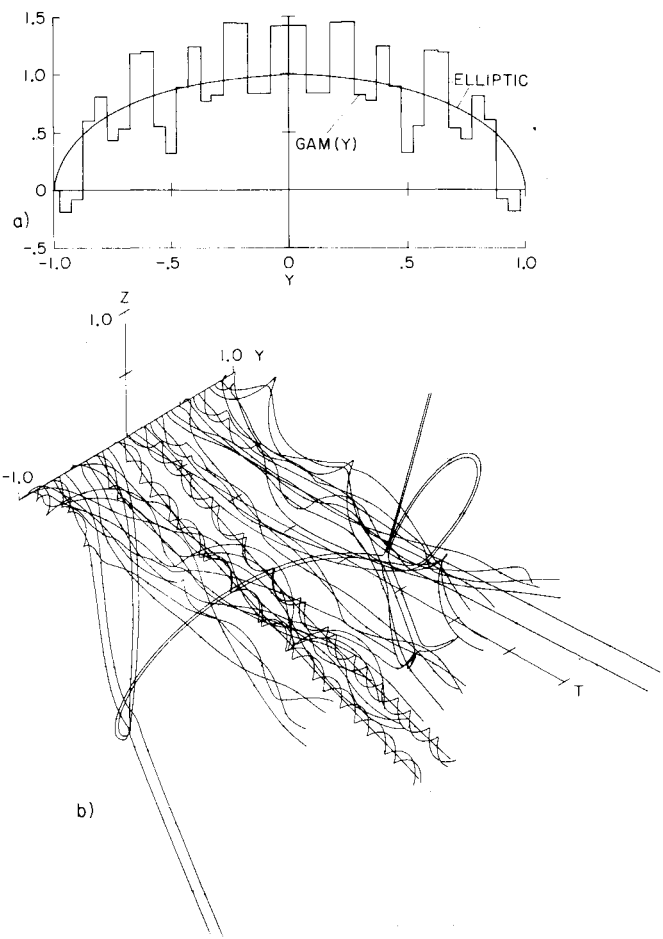

Fig. 14 Characteristic of wake of loading in Fig. 13 when sawtooth array of $\Delta\gamma = 0.4\Gamma_o$ has been added. When $b_g/b_f = 2$, $C_{l_r}/C_{L_a} = 0.13/\mathcal{R}_g$, a) Vortex array approximation to span loading; b) oblique view of vortices; $T_{max} = 2.8$.

are shown in Fig. 13. Note that fluctuations already exist in the loading as a result of the arrangement used for the flaps and pylons during landing. These built-in variations, however, must be supplemented with other spanwise variations to achieve sawtooth loading that is effective in randomizing the wake. As the proportion of sawtooth loading is increased, the wake system progresses from an orderly rollup into the somewhat random system shown in Fig. 14. A greater proportion of sawtoothing and a greater number of segments would, of course, produce a more chaotic wake. The loading that can be achieved with a given wing flap system will determine the amount and frequency of the sawtooth loading. It will then be necessary to investigate various combinations of flap settings for the kinds of loadings possible and to then calculate the resulting vortex wake to determine which configuration produces the least hazardous wake.

Some preliminary tests conducted by Ciffone and Orloff[23] indicate that the theoretical predictions made here are correct qualitatively. Although rolling moments on an encountering wing were not measured, it was found that the peak circumferential velocity in the vortices shed by tailored loading was reduced, and that a sawtooth loading led to random excursions of the vortices in the wake.

III. Conclusions

A theoretical study has been made of whether the rolling-moment hazard in a lift-generated wake could be reduced by suppressing the rollup of the vortex sheet shed by the span loading. For this purpose, the circulation distribution in two hypothetical wakes was first derived so that one would rotate and the other translate as a unit. Numerical calculations were then made of the inviscid motion of arrays of vortices used to represent these wakes and of the wakes of several span loadings constructed with the special arrays. The accuracy of these results was monitored so that the plotted results are reliable. Furthermore, the radial distribution of the circulation in the wake was compared and found to be in good agreement with the variation predicted by Betz' theory for tailored (rotating array) and elliptic loadings. A similar comparison could not be made for stepped loading (translating array) because that wake consists of a number of discrete vortices (rather than a single pair) that move in a chaotic way. These vortex excursions are desirable in that they cause the wake structure to disperse.

The rolling-moment coefficient estimated for a wing embedded in the wake shed by tailored loading indicates that the hazard is reduced for following wings with small but not intermediate or large spans. However, a substantial reduction in rolling moment is predicted for wings that encounter the wakes that trail from span loadings with a sawtooth character. These wakes contain several positive and negative vortices (rather than a single pair) which are needed to produce erratic motions that diffuse the vorticity. These predicted motions have been observed behind a wing with a sawtooth-type loading tested in a water tank.[23] The present study suggests that these span loading concepts be explored further to determine whether the wake-vortex hazard can be reduced to an acceptable level with reasonable flap settings on the generating wing.

Appendix : On the Interpretation of Wake Calculations

The time-dependent method used here to estimate the downstream structure of vortex wakes has two principal areas of difficulty. The first is to assess the numerical accuracy of the calculations and the second is to interpret the results. This appendix discusses these points and presents an approximate method for interpreting vortex-wake results in terms of rolling moment on an encountering wing.

Background

The use of an array of two-dimensional vortices to represent a continuous vortex sheet was introduced by Rosenhead[12] and

then applied by Westwater[13] to the rollup of an elliptically loaded wing. Westwater noted that error sources are introduced by the finite number of vortices used to replace the continuous sheet and by the step-by-step numerical calculations. He then noted that the results provide an idea of the form of the continuous sheet and that the numerical method gives a good approximation to the motion. He also noted that the finite number of vortices cannot represent the spiral form of the vortex sheet at its edges as predicted by Kaden.[14] Since that time, this time-dependent method has been used extensively to study the vortex wakes shed by wings. Several papers have also been written to elaborate on the shortcomings of the method and to introduce ways to remedy these shortcomings (e.g., Refs. 15–21). These discussions generally agree with Westwater in that the spiral shape at the edges of vortex sheets is often not well simulated by the vortex array and that the point vortices sometimes undergo excursions believed to be associated with the vortex array and not with the vortex sheet being represented.

Several methods have been introduced recently[19–21] to stabilize these vortex motions and to eliminate the excursions believed not to be a part of the vortex-sheet structure. Although these techniques suppress vortex excursions and sheet kinking, they also introduce another error source. The use of finite cores in the vortices suggested by Chorin and Bernard[19] and Kuwahara and Takami[20] or the accumulation of vortices at the center of the spiral as suggested by Moore[21] all contain arbitrary parameters that are not related to the conservation equations for the fluid they are to represent. The computed results may then appear more reasonable than those obtained from point vortices, but the quantitative accuracy is uncertain. As pointed out in the text, finite vortex cores instead of point vortices were used in a few cases to duplicate cases presented here and the vortex motions were smoothed. The qualitative nature of the solutions was not changed, however, if the core radius chosen for the vortices is less than the initial spacing. It was also found that the vortex motions depend on the core size chosen and the error monitors indicate significant error growth during a computation. These results were not included here because the character of these calculations is not greatly different, and an accurate estimate of the numerical error growth (see next section) could not be obtained for the cases with finite cores.

Numerical Accuracy

The motion of a number of two-dimensional point vortices in an incompressible fluid is an elliptic problem for which numerical calculations are known to be unstable so that any initial error grows with each time step. For this reason, the calculations are usually begun with a large number of significant figures (double precision on most computers) in the hope that the desired result can be achieved before accumulated errors wipe out all the accuracy. This was also done here. It is also essential that the accuracy or error accumulation be monitored during the calculations so that an inappropriate choice of mesh size or excessive error growth is detectable. For example, Westwater[18] used the first moment of vorticity as an indicator of accuracy. When suitable error monitors are used, it is possible to determine whether seemingly unrealistic results are attributable to numerical error or to properties of the vortex array being analyzed.

Three error monitoring parameters were used in the present analysis: 1) The first moments of vorticity for each side (to reduce the likelihood of compensating errors due to symmetry):

$$\bar{y}\Gamma_{\mathfrak{C}} = \bar{y}\sum_{j=1}^{N/2}\gamma_j = \sum_{j=1}^{N/2} y_j\gamma_j \qquad \text{(A1)}$$

2) The second moment of vorticity about the center of gravity for the vortices on each side:

$$J = \sum_{j=1}^{N/2}\left[(y_j-\bar{y})^2+(z_j-\bar{z})^2\right]\cdot\gamma_j \qquad \text{(A2)}$$

3) The Kirchhoff-Routh path function[22] for the entire array of vortices:

$$Wr = \sum_{i=1}^{N-1}\sum_{j=i+1}^{N}\left(\frac{\gamma_i\gamma_j}{4\pi}\right)\ln\left[(y_i-y_j)^2+(z_i-z_j)^2\right] \qquad \text{(A3)}$$

Note that none of these quantities is used in the time-dependent calculations nor do they depend on the numerical integration scheme used. They are evaluated every so many steps (usually every 10th or 20th) to ascertain how much error has accumulated in the positions of the assembly of vortices. As expected, during the calculations, the various parameters did indicate an error growth that reduces the number of significant figures. When the third significant figure (plotting accuracy) of any of the monitored quantities was affected, the calculations were terminated. If a large change occurred in the error monitors between steps in the calculations, it could usually be traced to unwarranted vortex excursions that could be cured by use of another mesh size. Hence, if the constraints are satisfied, as they were in all numerical results presented, the plotted results correctly represent the motion of vortices in the array. However, some of these motions may be associated only with the array of point vortices and may not be identified with the vortex sheet being represented. Past experience indicates, however, that gross aspects and trends of the vortex sheet are modeled correctly, but that, as with many finite-difference methods, the detailed motions are not always properly or adequately represented.

Note that the wake shed by tailored span loading is a continuous vortex sheet for each side of the wing. The stepped, sawtooth, and combined loadings, however, are vortex arrays and not continuous vortex sheets. For this reason, they are shown as spanwise discontinuous in the figures to indicate their discrete character. In practice, the steps in the loading are rounded, but the steps should be large enough and shaped so that the wake shed by the undulations in the loading quickly rolls up into an array of vortices. The numerical results for such vortex arrays should then be representative of the wake and should not be reinterpreted in terms of a continuous vortex sheet.

Estimate of Rolling Moment from Vortex Positions

A method is derived here for estimating the rolling moment on a wing that encounters a vortex wake when the wake structure has been determined by time-dependent calculations that used discrete vortices. The distribution of point vortices is first reinterpreted as a stepwise radial distribution of circulation about the centroid of vorticity for one side of the wing. This is done by assuming that the vorticity associated with a point vortex in the array is spread uniformly on a ring with a radius equal to the distance of the vortex from the centroid. As indicated in Figs. 6 and 10, the resulting stepwise curve for circulation as a function of radius agrees quite well with the variation predicted by Betz' theory[11] for both tailored and elliptic loading. These curves could be used to determine the circumferential velocity distribution in the vortex and then to estimate the torque, but some simplification can be achieved by placing the encountering wing at the centroid of vorticity and then calculating the torque using strip theory.

The rolling-moment coefficient is defined as

$$C_{l_f} = \text{torque}/(\tfrac{1}{2}\rho U_\infty{}^2 S_f\, b_f) \qquad \text{(A4)}$$

where S_f and b_f are the planform area and span of the following or encountering aircraft. The torque is estimated using the so-called strip theory wherein the lift on each spanwise element of the wing is assumed to be equal to the local two-dimensional value; i.e., $C_{L\alpha} = 2\pi$.

$$\text{torque} = \int_{-b_f/2}^{b_f/2} 2\pi\sin\alpha\cdot\tfrac{1}{2}\rho U_\infty{}^2 c_f\, y\, dy$$

where α is the local flow angle relative to the wing local chord, c_f, given by $\sin\alpha \approx w/U_\infty$. Since the wing center is located at the centroid of vorticity, the flow inclination can be written as

$$w/U_\infty = v_\theta/U_\infty = \Gamma_v(r)/2\pi r U_\infty$$

where the radius in the vortex and lateral distance on the wing are now the same. The rolling-moment coefficient for a flat rectangular wing ($c_f = S_f/b_f$) then becomes

$$C_{l_f} = 2(b_g/b_f)^2 \int_o^{\frac{1}{2}(b_f/b_g)} \left[\frac{\Gamma_v(r)}{b_g U_\infty}\right] d\left(\frac{r}{b_g}\right) \qquad (A5)$$

where b_g is the span of the generating wing and, as mentioned previously, $\Gamma_v(r)$ is the stepwise distribution of circulation in the vortex determined from the time-dependent calculations.** This expression resembles that for the lift on the generating wing when it is written as

$$C_{L_g} = 4\,\mathcal{R}_g \int_o^{1/2} \left[\frac{\Gamma_g(y)}{b_g U_\infty}\right] d\left(\frac{y}{b_g}\right) \qquad (A6)$$

where $\mathcal{R}_g$ is the aspect ratio and $\Gamma_g(y)$ is the spanwise bound circulation on the generating wing.

Since it is of interest to retain the lift on the generator aircraft while reducing the rolling moment hazard on a following or encountering aircraft, one hazard parameter than can be defined is the ratio of the moment on the follower to the lift on the generator, that is,

$$\text{hazard parameter} = C_{l_f}/C_{L_g} \qquad (A7)$$

When this parameter is evaluated for elliptic loading (with $b_g/b_f = 2$),

$$(C_{l_f}/C_{L_g})_{\text{elliptic}} = 1.413/(\Gamma_{\text{℄}}/b_g U_\infty)]/(\pi \mathcal{R}_g/2)(\Gamma_{\text{℄}}/b_g U_\infty)$$
$$= 0.9/\mathcal{R}_g$$

The corresponding value for a wing with rectangular loading is

$$(C_{l_f}/C_{L_g})_{\text{rect}} = (b_g/b_f)(\Gamma_{\text{℄}}/b_g U_\infty)/(2\,\mathcal{R}_g \Gamma_{\text{℄}}/b_g U_\infty)$$
$$= 1/\mathcal{R}_g$$

where $\Gamma_{\text{℄}}$ is the bound circulation at the center of the generating wing. Since most subsonic transport aircraft land at about the same speed, the reference velocity is assumed to be the same for both the generator and follower aircraft.

References

[1] Corsiglia, V. R., Jacobsen, R. A., and Chigier, N., "An Experimental Investigation of Trailing Vortices Behind a Wing with a Vortex Dissipator," *Aircraft Wake Turbulence*, edited by J. H. Olsen, A. Goldburg and M. Rogers, Plenum Publishing Corp., New York, Sept. 1970, pp. 229–242.

[2] Bilanin, A. J. and Widnall, S. E., "Aircraft Wake Dissipation by Sinusoidal Instability and Vortex Breakdown," AIAA Paper 73-107, Washington, D.C., 1973.

[3] Rorke, J. B., Moffitt, R. C., and Ward, J. F., "Wind Tunnel Simulation of Full Scale Vortices," A.H.S. Preprint 623, 28th Annual National Forum of the American Helicopter Society, Washington, D.C., May 1972.

[4] El-Ramly, Z., "Aircraft Trailing Vortices—a Survey of the Problem," Tech. Rept. ME/A 72-1, Nov. 1972, Carleton University, Ottawa, Canada.

[5] Hackett, J. E. and Evans, M. R., "Vortex Wakes Behind High-Lift Wings," *Journal of Aircraft*, Vol. 8, No. 5, May 1971, pp. 334–340.

[6] Scheiman, J. and Shivers, J. P., "Exploratory Investigation of the Structure of the Tip Vortex of a Semispan Wing for Several Wing-Tip Modifications," TN D-6101, Feb. 1971, NASA.

[7] Clements, R. R. and Maull, D. J., "The Rolling Up of a Trailing Vortex Sheet," *Aeronautical Journal*, Vol. 77, No. 745, Jan. 1973, pp. 46–51.

[8] Rehback, C., "Numerical Study of the Influence of the Wing-Tip Shape on the Vortex Sheet Rolling Up," TT F-14, 538, Aug. 1972, NASA.

[9] Rorke, J. B. and Moffitt, R. C., "Wing Tunnel Simulation of Full Scale Vortices," CR-2180, March 1973, NASA.

[10] Brown, C. E., "Aerodynamics of Wake Vortices," *AIAA Journal*, Vol. 11, No. 4, April 1973, pp. 531–536.

[11] Rossow, V. J., "On the Inviscid Rolled-Up Structure of Lift-Generated Vortices," *Journal of Aircraft*, Vol. 10, No. 11, Nov. 1973, pp. 647–650.

[12] Rosenhead, L., "The Formation of Vortices from a Surface of Discontinuity," *Proceedings of the Royal Society*, London, Vol. A134, 1931, pp. 170–192.

[13] Westwater, F. L., "The Rolling Up of the Surface of Discontinuity Behind an Aerofoil of Finite Span," Aeronautical Research Council, London, Repts. and Memo. 1692, 1935, pp. 116–131.

[14] Kaden, H., "Aufwicklung einer Unstabilen Unstetigkeitsfläche," *Ingenieur-Archiv.*, Bd. II, 1931, pp. 140–168.

[15] Spreiter, J. R. and Sacks, A. H., "The Rolling-Up of the Trailing Vortex Sheet and Its Effect on the Downwash Behind Wings," *Journal of the Aeronautical Sciences*, Vol. 18, No. 1, Jan. 1951, pp. 21–32.

[16] Hama, F. R. and Burke, E. R., "On the Rolling-Up of a Vortex Sheet," Tech. Note BN-220, AFOSR-TN 60-1069, Sept. 1960, Univ. of Maryland, College Park, Md.

[17] Takami, H., "A Numerical Experiment with Discrete-Vortex Approximation, with Reference to the Rolling Up of a Vortex Sheet," Sudaer 202 (AFOSR 64-1536), Sept. 1964, Univ. of Maryland, College Park, Md.

[18] Moore, D. W., "The Discrete Vortex Approximation of a Vortex Sheet," Rept. AFOSR-1084-69, Oct. 1971, Calif. Inst. of Tech., Pasadena, Calif.

[19] Chorin, A. J. and Bernard, P. S., "Discretization of a Vortex Sheet, with an Example of Roll-Up," Rept. FM-72-5, Nov. 1972, College of Engineering, Univ. of Calif., Berkeley, Calif.

[20] Kuwahara, K. and Takami, H., "Numerical Studies of Two-Dimensional Vortex Motion by a System of Point Vortices," *Journal of the Physical Society of Japan*, Vol. 34, No. 1, Jan. 1973, pp. 247–253.

[21] Moore, D. W., "A Numerical Study of the Roll-Up of a Finite Vortex Sheet," *Journal of Fluid Mechanics*, Vol. 63, Pt. 2, April 1974, pp. 225–235.

[22] Lin, C. C., "On the Motion of Vortices in Two Dimensions," No. 5, Applied Mathematics Series, The Univ. of Toronto Press, Toronto, Canada, 1943.

[23] Ciffone, D. L. and Orloff, K. L., "Far-Field Wake-Vortex Characteristics of Wings," AIAA Paper 74-505, Palo Alto, Calif., 1974.

[24] Lamb, H., *Hydrodynamics*, Dover, New York, N.Y., 1945, p. 232.

** The flux of angular momentum in the vortex is given by

$$F = \text{flux of angular momentum} = \int_o^r (2\pi r)\rho U_\infty v_\theta\, r\, dr$$

or, in dimensionless form,

$$F/(\tfrac{1}{2}\rho U_\infty{}^2 S_f b_f) = 2(b_g/b_f)^2 \int_o^{r/b_g} (r/c_f)[\Gamma_v(r)/b_g U_\infty]\, d(r/b_g)$$

Comparison with Eq. (A5) indicates that the torque estimated by strip theory for $r < c_f$ exceeds the maximum possible from angular momentum considerations. Therefore, the rolling-moment estimate by Eq. (A5) will be greater than expected in an experiment unless other compensating effects occur.